Low-Dimensional Materials
https://www.sciltp.com/journals/ldm

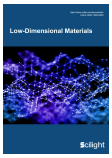

Supplementary Materials

Ultrathin ZnS Electron Transport Layer Enables Efficient p-Si Photocathode for Photoelectrochemical Hydrogen Production

Yanming Li [1,†], Jianjun Jiang [1,†], Chenglong Ding [1], Hao Wang [1], Yequan Xiao [2,*], Jingfu He [1,*] and Changli Li [1,*]

[1] School of Materials, Shenzhen Campus of Sun Yat-sen University, Shenzhen 518107, China
[2] Hubei Provincial Engineering Research Center for Solar Energy High-value Utilization and Green Conversion, College of Materials Science and Engineering, China Three Gorges University, Yichang 443002, China
* Correspondence: xiaoyequan@ctgu.edu.cn (Y.X.); hejf27@mail.sysu.edu.cn (J.H.); lichli5@mail.sysu.edu.cn (C.L.)
† These authors contributed equally to this work.

Experimental Section

Deposition of ZnS Film by Sputtering

ZnS ultra-thin films with different thickness were deposited on cleaned p-Si substrates by a facile magnetron sputtering method. Firstly, *p*-type silicon (300 ± 10μm thickness, 1–5 Ω·cm resistivity, (100) oriented, Suzhou Resemi Semiconductor Co., Ltd., Suzhou, China) was cut into small pieces (~1 × 1 cm^2), then went through a standard RCA cleaning procedure and dried with N_2. Then, ZnS thin films with different thicknesses were sputtered on cleaned p-Si substrates by sputtering ZnS target (99.9% purity, 60 × 3 mm with bonding Cu, Beijing Jing Mai Zhong Ke Material Technology Co., Ltd., Beijing, China) using magnetron sputtering equipment (CK400, Shenyang Topa Technology Co., Ltd., Shenyang, China). During the whole sputtering process, the power is fixed at 30 W, the Ar flow rate is kept at 25 sccm, the working pressure is set as 1.0 Pa, the deposition rate of ZnS is ~1.7 Å/s. After sputtering, samples (p-Si/ZnS) were removed in a home-made double heating source tube furnace for further sulfidation or annealing.

Deposition of CdS, In_2S_3, MoS_2 Film by Sputtering

CdS, In_2S_3, MoS_2 films were deposited on cleaned p-Si substrates by magnetron sputtering. The purity and manufacturer of the target are the same as above. The sputtering parameters referred to above. The deposition rate of CdS, In_2S_3, and MoS_2 is ~1.7 Å/s, 1.0 Å/s, and 1.2 Å/s, respectively. The thickness of three films is ~40 nm. After sputtering process, samples (p-Si/CdS, p-Si/In_2S_3, and p-Si/MoS_2) were removed in a home-made double heating source tube furnace for sulfidation.

Deposition of Pt Layer by Sputtering

Pt films were deposited on ZnS-coated Si surface by magnetron sputtering. The sputtering conditions were as follows: base vacuum of 5 × 10^{-4} Pa, sputtering power of 30 W, Ar flow rate of 25 sccm, working pressure of 1.0 Pa, room temperature substrate, deposition rate of 0.1 nm·s^{-1}, and a total deposition time of 10 s. The film thickness was monitored using the SI-TM508 quartz crystal microbalance.

Sulfidation Process of n-Type Buffers

The sulfidation process is based on a home-made double temperature zone tube furnace. On the basis of the purchased tubular furnace (OTF-1200X, Hefei Kejing Material Technology Co., Ltd., Hefei, China), glass fiber heating belt is wound 40 cm away from the center of the tube furnace to create another heating source (Schematic diagram of sulfidation is shown in Figure S1). High purity S powder (>99.99% purity, Beijing Jing Mai Zhong Ke Material Technology Co., Ltd., Beijing, China) is placed in the center of the heating belt as a sulfur source, and

the sample is placed in the middle of the tube furnace. Ar flow rate of 600 sccm is introduced to the tube for more than 30 min to eliminate possible oxygen. During the sulfidation process, Ar flow rate is kept at 600 sccm, the temperature of S powder (Glass fiber heating belt) is fixed at 200 ℃. Changing the setting of tube furnace to explore the influence of sulfidation temperature on PEC performance. For the annealing process, the difference is that glass fiber heating belt is not turned on throughout the whole process. After sulfidation or annealing process, samples were transferred to magnetron sputtering system to deposit Pt catalyst.

Fabrication of Si-Based Photocathode

Pt catalyst was initially deposited on samples by magnetron sputtering. After the deposition, scraping InGa alloy (>99.99% purity, Dongguan chemical reagent) on the back of silicon wafer to build ohmic contact. Using silver paste (05001-AB, SPI supplies) to connect Si substrate with Cu wire. The back and side of the electrode are wrapped with acid and alkali resistant epoxy resin. Using ImageJ software to acquire effective working area of electrode (~0.1–0.5 cm^2).

Photoelectrochemical Measurements

The PEC measurements were carried out using three-electrode cell configuration (a Pt wire as the counter electrode, an Ag/AgCl electrode as the reference electrode) in the pH 5.7 phosphate buffer (containing 0.5 M Na_2SO_4, 0.25 M Na_2HPO_4, and 0.25 M NaH_2PO_4, >99.9% purity of all reagents, Aladdin) with magnetic stirring and N_2 purging. Potentials of these PEC measurements that referred to the Ag/AgCl electrode ($V_{Ag/AgCl}$) were converted to those that referred to the reversible hydrogen electrode (V_{RHE}) by using the following equation:

$$V_{RHE} = V_{Ag/AgCl} + 0.059 \times pH + 0.197 \quad \text{(S1)}$$

A commercial AM 1.5 G solar simulator (100 $mW.cm^{-2}$, LCS-100, Newport Corporation, 94011A-ES) was employed as simulated sunlight. The onset potential is defined as the potential at which the photocurrent density reaches −0.1 mA cm^{-2} under AM 1.5 G illumination [1,2]. To measure the barrier height of p-Si/ZnS, Mott-Schottky test was carried out in 0.5 mM/0.5 mM $K_3Fe(CN)_6/K_4Fe(CN)_6$ in 1 M KCl. The test was employed through three-electrode cell configuration (a Carbon rod as the counter electrode, a Pt sheet electrode as the reference electrode) with 5 mV AC voltage signal at a frequency of 10 kHz. To know the flat-band potential and charge carrier density, Mott-Schottky test was carried out using a 5 mV AC voltage signal at a frequency of 2 kHz in 0.5 M Na_2SO_4 (a Pt sheet as the counter electrode, an Ag/AgCl electrode as the reference electrode). The flat-band potential and charge carrier density can be extracted from the x-intercept and slope of the plot between the reciprocal of the square of capacitance per unit area, $1/C^2$, versus the applied voltage, V, according to the Mott−Schottky equation [3,4]:

$$\frac{1}{C^2} = \frac{2}{e\varepsilon\varepsilon_0 N_D}\left[V - V_{fb} - \frac{K_B T}{e}\right] \quad \text{(S2)}$$

where e is the electronic charge, ε is the relative permittivity of different n-type buffers ($\varepsilon \sim 7.5$ for ZnS, $\varepsilon \sim 8.9$ for CdS, $\varepsilon \sim 13$ for In_2S_3, and $\varepsilon \sim 8.5$ for MoS_2) [5–7], ε_0 is the permittivity of vacuum, K_B is Boltzmann's constant, T is the absolute temperature, and N_D is the carrier density. The x-intercept of the linear region of the MS plot is indicative of the flat band potential V_{fb}. From the slope K_{MS} of the lines, carrier density N_D is estimated from the equation:

$$N_D = \frac{2}{e\varepsilon\varepsilon_0 K_{MS}} \quad \text{(S3)}$$

The barrier height (Φ_b), was then calculated using the following relation:

$$\Phi_b = -qV_{fB} + V_n$$

with V_n being the energy difference between the conduction band and the Fermi level, that was calculated using the following equation:

$$V_n = E_C - E_F = K_B T In \frac{N_C}{N_D} \quad \text{(S4)}$$

N_C, the effective density of states in conduction band which can be expressed as:

$$N_C = 2\left(\frac{2\pi m^* K_B T}{e^2}\right)^{3/2} \quad \text{(S5)}$$

where m^* is the effective electron mass of different *n*-type buffers (m^* ~ 0.28 for ZnS, m^* ~ 0.21 for CdS, m^* ~ 0.162 for In_2S_3, and m^* ~ 0.553 for MoS_2) [5,7,8].

The *ABPE* was calculated using the following equation:

$$ABPE = \frac{|J_{light}| \times [V_{RHE} - V_{H+/H2}]}{P_{light}} \quad \text{(S6)}$$

where J_{light} (mA/cm^2) is the photocurrent density at a specific applied potential. V_{RHE} is the applied potential versus *RHE*. $V_{H+/H2}$ is the thermodynamic potential for hydrogen evolution (0 V vs. *RHE*), and P_{light} is the power of simulated light (100 mW/cm^2).

Characterization

The structure of samples was characterized by X-ray photoelectron spectroscopy (Thermo-VG Scientific, ESCALAB 250), UV-VIS spectrum (PerkinElmer, Lambda950).

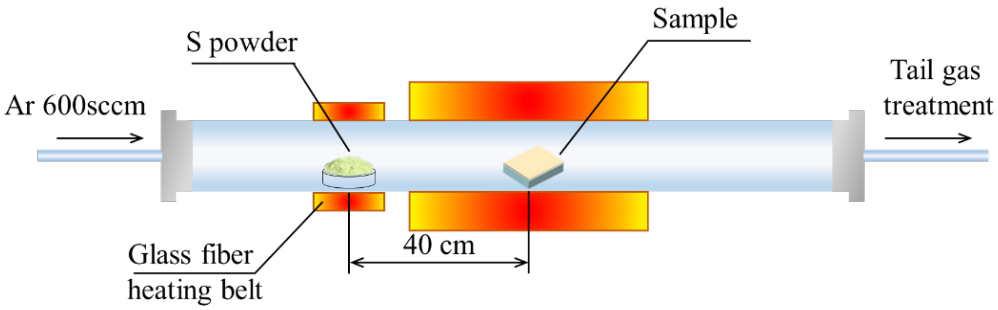

Figure S1. Schematic diagram of the sulfidation process.

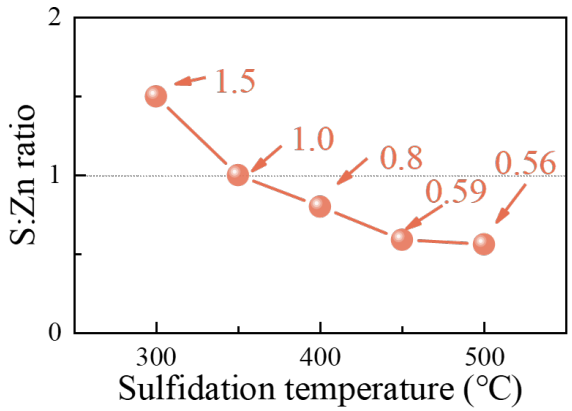

Figure S2. S:Zn ratio under different sulfidation temperatures.

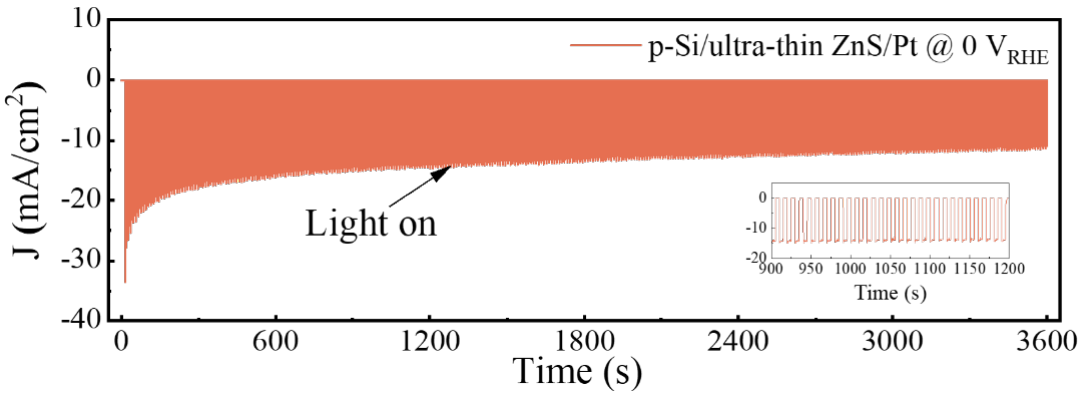

Figure S3. Stability test of p-Si/ZnS/Pt electrode after 400 ℃ sulfidation. The test was carried out in phosphate buffer (pH 5.7) under AM 1.5 G illumination, with applied voltage of 0 V_{RHE}.

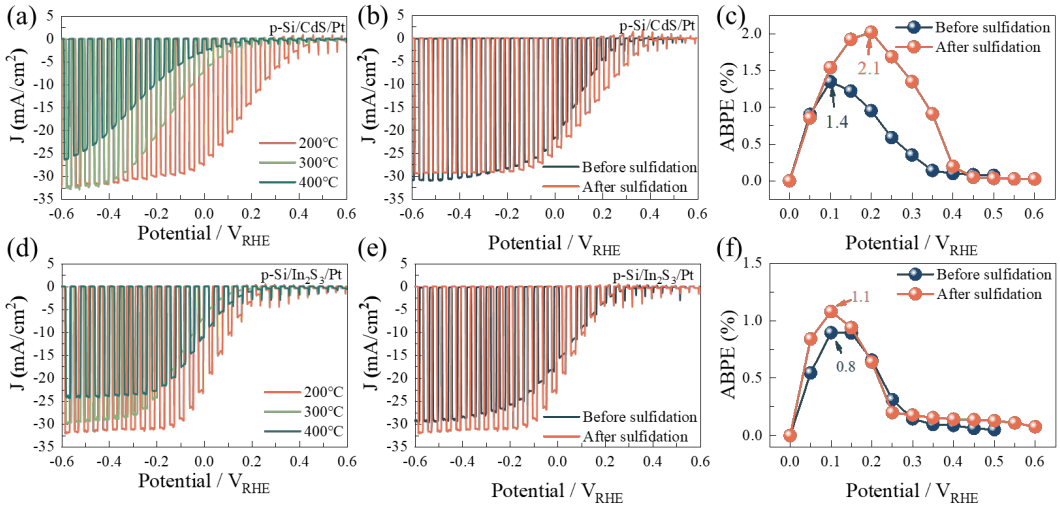

Figure S4. The effects of sulfidation treatment on the PEC performance of p-Si/CdS and p-Si/In_2S_3 photocathodes. (**a**,**d**) The influence of sulfidation temperature of p-Si/CdS and p-Si/In_2S_3 on PEC performance. (**b**,**e**) PEC performance comparison before and after the sulfidation process. (**c**,**f**) ABPE comparison of p-Si/CdS and p-Si/In_2S_3 before and after the sulfidation process.

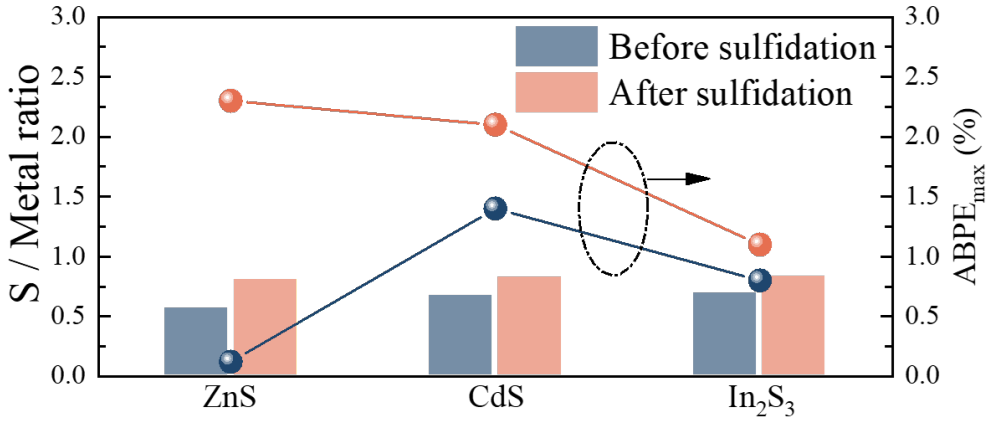

Figure S5. S:Zn ratio variation of the mentioned ETLs after sulfidation. The S content increased after sulfidation process for all buffers. Before the sulfidation process, the S:Metal ratio is 0.56, 0.67, and 0.69 for ZnS, CdS, and In_2S_3, indicating the unreasonable content of sulfur element. After the sulfidation process, this ratio increased to 0.80, 0.82, and 0.83.

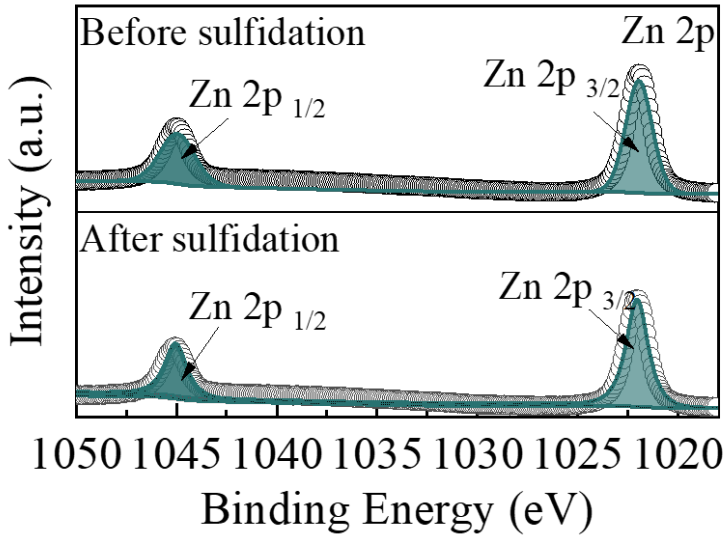

Figure S6. XPS binding energy variation of Zn 2p before and after sulfidation.

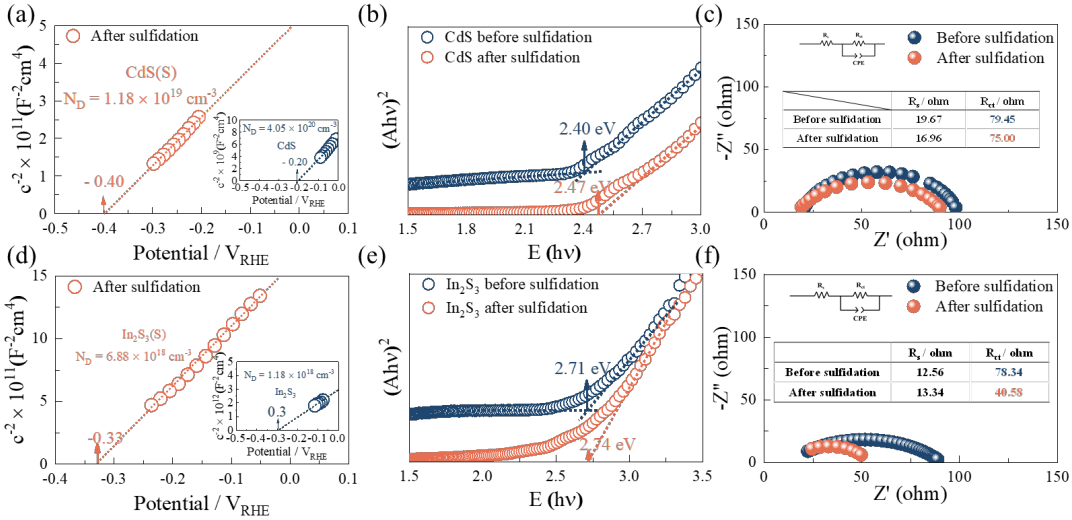

Figure S7. The electronic and interfacial property changes of p-Si/CdS and p-Si/In_2S_3 photocathodes before and after sulfidation. (**a**,**d**) Comparison of flat-band potential and carrier density of p-Si/CdS and p-Si/In_2S_3 before and after sulfidation. (**b**,**e**) Comparison of absorption band gap of p-Si/CdS and p-Si/In_2S_3 before and after sulfidation. (**c**,**f**) Comparison of electrochemical impedance spectroscopy of p-Si/CdS and p-Si/In_2S_3 before and after sulfidation, measured at 0 V_{RHE} under AM 1.5 G simulated sunlight irradiation in phosphate buffer.

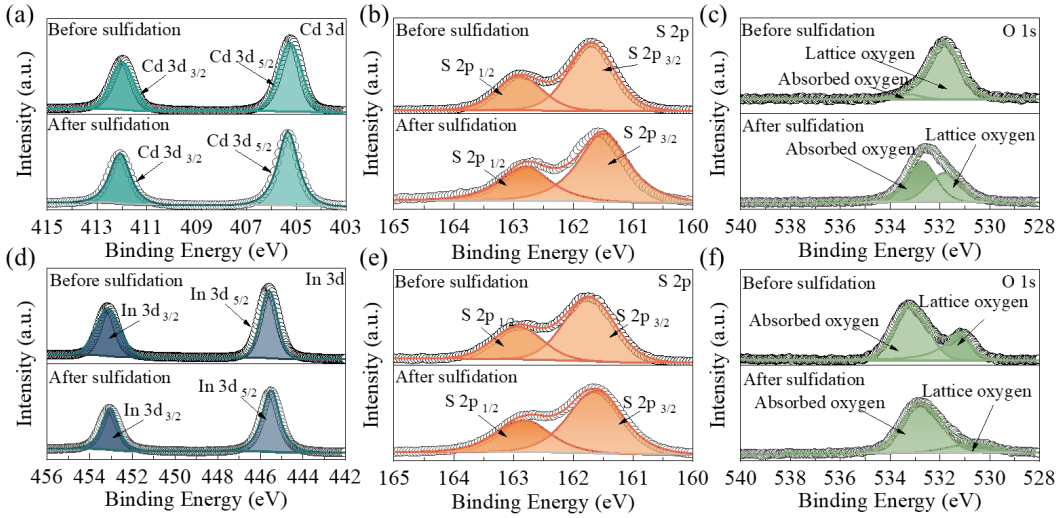

Figure S8. XPS binding energy variation before and after sulfidation. (**a**–**c**) CdS; (**d**–**f**) In_2S_3.

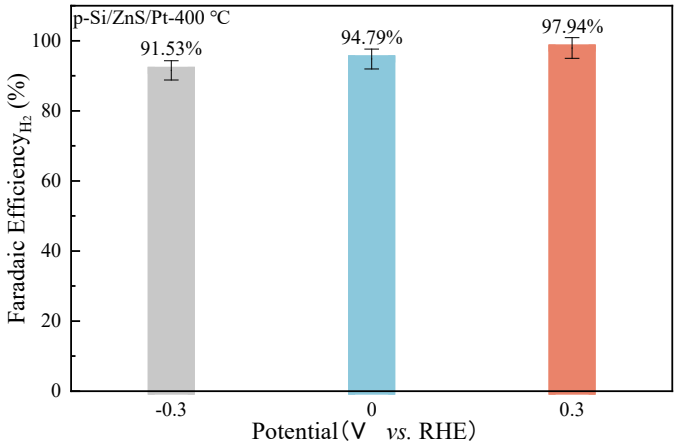

Figure S9. FE of the p-Si/ZnS/Pt-400 ℃ photocathode tested under 0.3 V, 0 V, and −0.3 V vs. RHE during PEC hydrogen evolution.

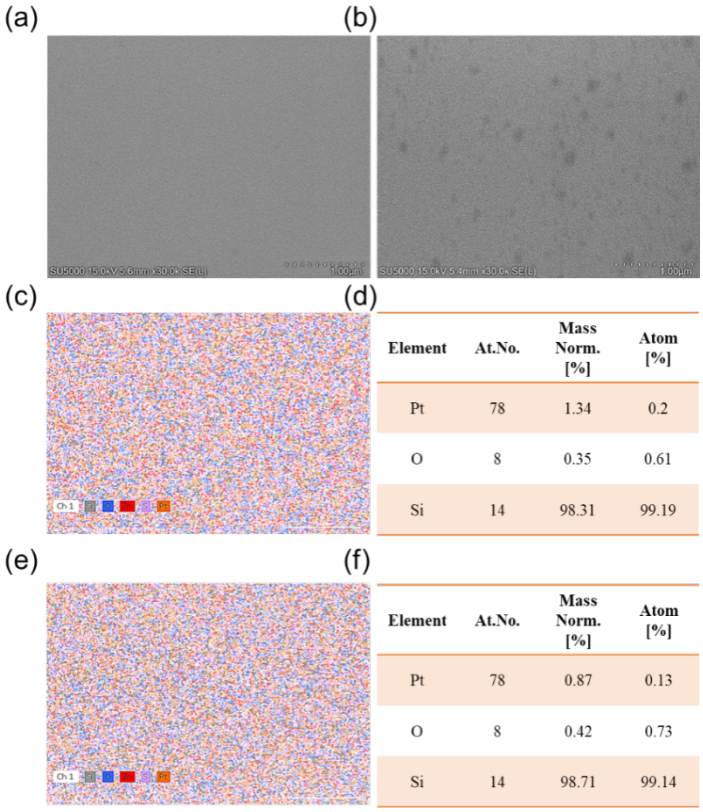

Element	At.No.	Mass Norm. [%]	Atom [%]
Pt	78	1.34	0.2
O	8	0.35	0.61
Si	14	98.31	99.19

Element	At.No.	Mass Norm. [%]	Atom [%]
Pt	78	0.87	0.13
O	8	0.42	0.73
Si	14	98.71	99.14

Figure S10. The morphology changes of the p-Si/ZnS/Pt-400 ℃ photocathode before (**a**) and after (**b**) PEC hydrogen evolution under 0 V vs. RHE for 1 h. The energy-dispersive X-ray spectroscopy (EDS) mapping images for the p-Si/ZnS/Pt-400 ℃ photocathode before (**c**,**d**) and after (**e**,**f**) PEC hydrogen evolution under 0 V vs. RHE for 1 h.

The EDS mapping results reveal that the Pt/O atomic ratio decreases from 1:3 to 1:5.6 after 1 h of operation, confirming significant Pt leaching. This degradation induces surface defects that promote charge recombination instead of effective carrier separation, leading to parasitic charge consumption and a gradual decline in photocurrent density.

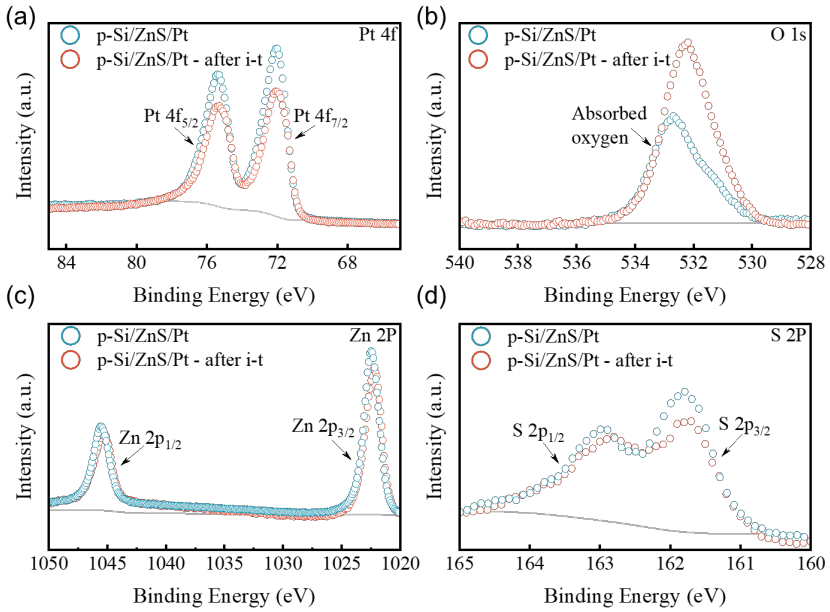

Figure S11. High-resolution XPS spectra of the p-Si/ZnS/Pt photocathode before and after 1 h PEC hydrogen evolution at 0 V vs. RHE. (**a**) Pt 4f; (**b**) O 1s; (**c**) Zn 2p; and (**d**) S 2p. Slight changes in Pt intensity and S:Zn ratio, along with increased O 1s signal, indicate partial Pt dissolution and minor surface reoxidation/stoichiometry changes in ZnS after operation.

The XPS survey and high-resolution spectra (Pt 4f, Zn 2p, S 2p, and O 1s) further confirm chemical changes after operation. The S:Zn ratio decreases slightly, and an increased O 1s signal indicates partial surface reoxidation of ZnS. The Pt 4f peak shows a small reduction in intensity, consistent with partial surface dissolution. We therefore attribute the ~34% photocurrent loss to a combination of (i) Pt nanoparticle detachment/dissolution and (ii) minor alteration in ZnS stoichiometry leading to additional surface defects and increased recombination.

References

1. Zhang, D.; Li, H.; Riaz, A.; et al. Unconventional Direct Synthesis of Ni_3N/Ni with N-Vacancies for Efficient and Stable Hydrogen Evolution. *Energy Environ. Sci.* **2022**, *15*, 185–195.
2. Zhang, D.; Pan, W.; Sharma, A.; et al. Over 14% Unassisted Water Splitting Driven by Immersed Perovskite/Si Tandem Photoanode with Ni-Based Catalysts. *Mater. Today Energy* **2025**, *48*, 101809.
3. Loget, G.; Mériadec, C.; Dorcet, V.; et al. Tailoring the Photoelectrochemistry of Catalytic Metal-Insulator-Semiconductor (MIS) Photoanodes by a Dissolution Method. *Nat. Commun.* **2019**, *10*, 3522.
4. Li, Y.; Ding, C.; Li, Y.; et al. Engineering the Inhomogeneity of Metal–Insulator–Semiconductor Junctions for Photoelectrochemical Methanol Oxidation. *ACS Appl. Mater. Interfaces* **2023**, *15*, 59403–59412.
5. Streetman, B.G.; Banerjee, S. *Solid State Electronic Devices New Jersey*; Prentice Hall: Upper Saddle River, NJ, USA, 2000.
6. Wang, L.; Xia, L.; Wu, Y.; et al. Zr-Doped β-In_2S_3 Ultrathin Nanoflakes as Photoanodes: Enhanced Visible-Light-Driven Photoelectrochemical Water Splitting. *ACS Sustain. Chem. Eng.* **2016**, *4*, 2606–2614.
7. Cheiwchanchamnangij, T.; Lambrecht, W.R. Quasiparticle band structure calculation of monolayer, bilayer, and bulk MoS_2. *Phys. Rev. B Condens. Matter Mater. Phys.* **2012**, *85*, 205302.
8. Zhao, Z.; Cao, Y.; Yi, J.; et al. Band-Edge Electronic Structure of β-In_2S_3: The Role of s or p Orbitals of Atoms at Different Lattice Positions. *ChemPhysChem* **2012**,*13*, 1551–1556.